International Journal of Robotics and Control Systems
Vol. 4, No. 2, 2024, pp. 910-928
ISSN 2775-2658
http://pubs2.ascee.org/index.php/ijrcs

Robust Voltage Control of a Single-Phase UPS Inverter Utilizing LMI-Based Optimization with All-Pass Filter Under System Uncertainty

Heng Tang [a,b,1], Chivon Choeung [a,2,*], Sarot Srang [c,3], Bunne So [a,4], Socheat Yay [a,5], Panha Soth [a,6], Horchhong Cheng [a,7]

[a] Faculty of Electricity, National Polytechnic Institute of Cambodia, Phnom Penh 120901, Cambodia
[b] Graduate School, National Polytechnic Institute of Cambodia, Phnom Penh 120901, Cambodia
[c] Industrial and Mechanical Engineering, Institute of Technology of Cambodia, Phnom Penh 120408, Cambodia
[1] tangheng@npic.edu.kh; [2] choeungchivon@npic.edu.kh; [3] srangsarot@itc.edu.kh; [4] sobunne@npic.edu.kh; [5] yaysocheat@npic.edu.kh; [6] sothpanha@npic.edu.kh; [7] horchhong@gmail.com
* Corresponding Author

ARTICLE INFO

Article history
Received May 02, 2024
Revised June 10, 2024
Accepted June 13, 2024

Keywords
Single-Phase Inverter;
Linear Matrix Inequality;
Uncertainty Model;
All-Pass Filter;
State Feedback Control;
Integral Control;
Digital Signal Processor

ABSTRACT

This paper proposes a systematic control design for a single-phase LC-filtered inverter considering uncertain system parameters. One major difficulty in controlling single-phase power converters is the lack of a direct conversion method for transforming single-phase signals into dq-frame signals. By employing an all-pass filter in this proposed approach, it is possible to control the output voltage in terms of DC quantity or the dq-rotating frame. Furthermore, voltage stability and harmonic distortion (THD) minimization of the uninterruptible power supply (UPS) are major concerns in inverter design. Therefore, this controller uses integral action to get rid of steady-state errors and stabilize the closed-loop system by the state feedback control. In order to enlarge and guarantee the stability range in the presence of potential parameter fluctuations, an uncertainty model is being considered. In this context, the uncertainty models refer to the potential model with variations in the filter's inductance and capacitance caused by operating temperature, aging, and various external factors. The efficacy of the control approach is assessed through simulations and experiments, with the objective of comparing its results with those of the PI control using a control board featuring a TMS320F28335 digital signal processor. Consequently, the proposed approach offers lower THD at every load step with lesser afford in performance tuning in comparison to the PI method.

1. Introduction

Uninterruptible power supply (UPS) is essential in maintaining electrical power during unexpected outages or interruptions, ensuring that critical equipment and systems remain operational. The inverters inside UPS system convert DC power from a battery or other source into AC power, allowing for seamless transitions during power failures [1]. A good inverter must provide a well-regulated output voltage with robust stability under various types of conditions. Voltage stability in single-phase inverters for UPS is a critical factor in ensuring the reliable operation of sensitive

electronic equipment. When the input voltage fluctuates or drops below a certain threshold, the inverter must be able to quickly and accurately regulate the output voltage to maintain a stable power supply. This is especially important in applications where even a momentary loss of power could result in data loss or equipment damage. Overall, UPS single phase inverters play a crucial role in protecting sensitive electronics and ensuring uninterrupted power supply in various applications. Thus, many control methods have been proposed for single-phase inverters to provide voltage stability and good reference tracking performances.

Deadbeat control has been presented in [2]-[4] for UPS inverters. The term “deadbeat” signifies the system's ability to “beat” or completely eliminate the error in a finite number of steps, leading to a “dead” or zero error state very quickly. These techniques offer a rapid transient response, allowing the system's output to reach a steady state in only a few sampling steps. Based on a predictive regulator on both output voltage and inductor current, a digital control method for the inverter stage of UPSs is proposed in [5]. Another deadbeat control method has been studied in [6] for a three-phase, three-level T-type inverter that is equipped with an output LC-filter. This control technique is specifically designed for UPS applications. A method discussed in [7] proposes a deadbeat control strategy that incorporates disturbance compensation. This control method utilizes a 1 MHz multisampling technique for three-phase pulse-width modulated inverter systems. Simulation and experiment demonstrate that the resistance to load variation is superior to that of the traditional deadbeat control method. The work conducted by [8] focuses on a new deadbeat control technique for a three-phase grid-connected voltage source inverter (VSI) with an output LCL filter in the natural frame. The system model in the natural frame is obtained by incorporating an LCL filter at the output of the three-phase grid-connected VSI. The performance and feasibility of the proposed deadbeat control method are assessed in balanced, unbalanced, and distorted grid situations. To summarize, the abovementioned methods mostly focus on providing fast transient performance and noise compensation using disturbance observers. However, the effectiveness of these approaches may be compromised when the system's parameters deviate from the real values or when there is noise existing in the system. Disturbance observer is used in these methods to enhance the output which causes more complexity in control design.

Proportional-Integral (PI) control is essential in control systems as it effectively eliminates steady-state errors and enhances the system's response time. PI control is a control method that combines proportional and integral control actions to efficiently ensure stability and accuracy in a wide range of industrial applications. A study discussed in [9] uses PI and proportional resonance control to decrease harmonic current in photovoltaic grid-connected inverters for optimal dynamic response. In addition to PI control, [10] proposes the Enhanced Bacterial Forging Technique (EBFA), a novel intelligent computer technique, as an effective reactive power controller for OGHPS voltage management. The method proposed in [11] improved PI and repetitive controllers for dual-buck inverters. Furthermore, [12] designs a single-phase photovoltaic inverter using double closed-loop PI and quasi-PR control. The purpose of [13] is to develop quadratic boost converter inverter systems (QBCIS) and evaluate proportional integral (PI) and fractional order proportional integral derivative (FOPID)-based SVMI systems. A related study [14] devised a harmonic suppression strategy using repeated and PI control to address grid-connected current harmonics in solar grid-connected inverters. The inner loop has PI control and the outer loop repeated control to improve dynamic performance and harmonic suppression. In [15], multiple single-phase standalone inverter control techniques were compared. Different controllers used in freestanding single-phase photovoltaic (PV) inverters are compared. The single-phase standalone inverter's output depends on the proposed control methods. Added to that, [16] proposes a super-twisting algorithm to reject harmonic perturbations in renewable energy conversion systems. A super-twisting algorithm may reject harmonic disturbances on three-phase grid-tied inverters. In experimental configurations with PI control, inverter current distortion reaches 11.4%. Other notable works can be found in [17]-[19]. In summary, employing the PI controller in power converter control results in exceptional performance, eliminating any offset error. Nevertheless, a prevalent disadvantage of PI control is the need for considerable time spent fine-tuning to achieve the most optimal output.

Real-time power converter optimization using model predictive control (MPC) is very effective. MPC continually predicts system behavior and adjusts control inputs to optimize power converter efficiency, stability, and performance. Due to this reasons, a modified packed U-cell five-level inverter with an MPC method for a single-phase active power filter is proposed in [20]. Additionally, to integrate solar PV systems into the grid, a new inverter design with fewer switches and flying capacitors is introduced. This integration was carried out using model predictive control [21]. Moreover, a method proposed in [22] presents a self-governing model predictive-controlled smart PV inverter that anticipates and responds to grid disturbances. The proposed AMPC approach improves smart inverter performance. Similarly, a nine-switch inverter (NSI)-based MPC technique for AC driving systems is discussed in [23]. Three distinct Finite Control Set Model Predictive Control (FCS-MPC) strategies are introduced and explained in that paper. Meanwhile, to eliminate the common-mode voltage in a three-phase neutral-point-clamped inverter and track other control objectives, conventional model predictive control has been enhanced and transformed into supervised learning model predictive control [24]. The traditional quasi-Z inverter's typical PI control has parameter adjustment and hysteresis issues. Generally, traditional MPCs are slower and less precise in current management. The restricted switch state determines the output vector after converting the current to the dq coordinate system. This allows for tracking the reference current and implementing FCS-MPC [25]. In summary, MPC has the ability to enhance the effectiveness, reliability, and overall performance of the aforementioned power converters. However, model predictive control is constrained by the requirement for precise system dynamics modeling and the computational complexity of solving the real-time optimization problem. Furthermore, to address the offset error resulting from model mismatch, it is necessary to utilize disturbance observers, which even more increases the complexity of the MPC.

This study utilizes a robust control method for a single-phase inverter that features an output LC-filter. A key challenge in controlling single-phase power converters is the lack of a direct method for transforming single-phase signals into dq-frame signals. By utilizing an all-pass filter in this proposed method, it becomes achievable to regulate the output voltage with regard to the DC quantity or the dq-rotating frame. Moreover, ensuring voltage stability and minimizing THD are important priorities when designing a UPS inverter. As an additional point of interest, this paper is the expanded version of a proceeding [26] that includes the results of the experiments using TMS320F28335 digital signal processor. The TMS320F28335 is utilized for inverter control because of its powerful 32-bit DSP core, integrated floating-point unit, and numerous extensions such as pulse width modulation and analog to digital converter modules. These features allow for accurate and efficient control of power switches and real-time feedback. Moreover, the real-time control capabilities, comprehensive software support, and development tools provided by Texas Instruments make it a very suitable option for durable and adaptable inverter systems. The controller of this proposed approach utilizes state feedback with integral control to ensure stability and avoid steady-state error. In contrast to a traditional MPC, this proposed controller has the ability to eliminate an offset error in order to achieve accurate reference tracking. This study also includes the consideration of an all-pass filter, which is used to generate an artificial β-signal. This allows for the controller to be easily operated in a dq-synchronous frame. An optimization technique based on Linear Matrix Inequalities (LMI) is employed to calculate the stabilizing gains of the controllers. LMI is crucial in inverter control as it allows for the design of robust and optimal controllers using efficient convex optimization techniques, ensuring stability and performance under varying conditions [27]-[29]. The objective is to optimize the convergence rate to a steady state, even in the presence of uncertainties. The uncertainty models in this proposed method refer to the potential model with variations in the filter's inductance and capacitance caused by operating temperature, aging, and various external factors [30], [31]. As mentioned before, deadbeat control is really sensitive to noise and disturbances. To address this issue, uncertainty models in this proposed method enhance its performance by allowing for a broader range of stability, even when faced with uncertain practical values of the LC-filter. This is in contrast to deadbeat control, which does not offer the same level of adaptability. This method offers a systematic approach to controller design by minimizing the need for gain tuning compared to traditional PI controllers. The simulations

and experiments are conducted using different load steps to verify the robustness of the proposed method. Furthermore, a comparative analysis is conducted to verify the efficacy of robust control by comparing the output performance, particularly the THD, with that of the PI control. Both experimental results and simulations demonstrate that the proposed approach yields superior THD in comparison to PI control at every load step.

2. State Space Model

2.1. Phase-Shifting Using All-Pass Filter

An all-pass filter is a type of electronic filter that passes all frequencies of the input signal equally in amplitude but alters the phase relationship among various frequencies [32]. The primary function of an all-pass filter is to modify the phase of the input signal without affecting its amplitude. The phase shift introduced by the filter is a function of frequency. An all-pass filter's circuit can be found in Fig. 1. And its transfer function can be written as:

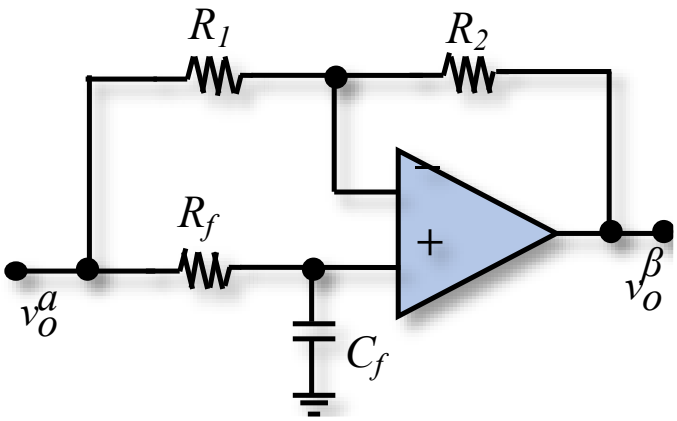

Fig. 1. All-pass filter incorporating with a low-pass filter

$$\frac{v_o^a(s)}{v_o^\beta(s)} = \frac{-R_f C_f s + 1}{R_f C_f s + 1} = \frac{-s + \omega_c}{s + \omega_c} \tag{1}$$

In this context, ω_c denotes the cut-off frequency of the all-pass filter and set to 100π rad/s which is the same as output voltage frequency. By applying Tustin's theory in the z-domain to (1), the discretized transfer function can be obtained as:

$$\frac{v_o^a[k]}{v_o^\beta[k]} = \frac{b_2 + b_1 z^{-1}}{b_1 + b_2 z^{-1}} \tag{2}$$

Here, $s = (2 - 2z^{-1})/(h + hz^{-1})$, $b_1 = \omega_c h + 2, b_2 = \omega_c h - 2$, and h is the sampling instance. Then, the output of the all-pass filter [32] can be obtained as:

$$v_o^\beta[k] = \frac{b_2}{b_1} v_o^a[k] + v_o^a[k-1] + \frac{b_2}{b_1} v_o^\beta[k-1] \tag{3}$$

By applying (3) the output of the AC voltage and current can be shifted 90 degrees from the original phase.

2.2. Single-Phase Inverter Model

The proposed single-phase inverter uses LC-filter to smooth the output waveform, reduce harmonics and electromagnetic interference, protect the load, and improve the overall efficiency of the inverter. The dynamic of the single-phase inverter in Fig. 2 can be obtained using Kirchoff's law as:

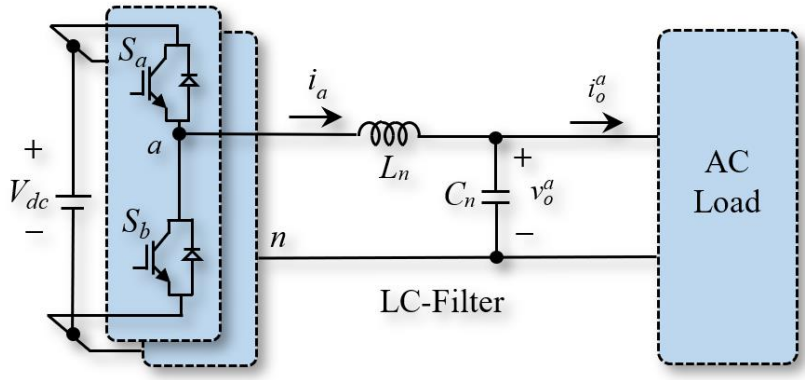

Fig. 2. Single-phase inverter with output LC-filter

$$i_o^a(t) = L_n^{-1}v^{an}(t) - L_n^{-1}v_o^a(t) \tag{4}$$

$$\dot{v}_o^a(t) = C_n^{-1}i^a(t) - C_n^{-1}i_o^a(t) \tag{5}$$

Where C_n denotes filter capacitance, $L_n$represents filter inductance, $i_o^a(t)$ is output current, $v_o^a(t)$ denotes output voltage, $i^a(t)$ is inductor current, and $v^{an}(t)$ represents the pole voltage. The inductor L_n opposes changes in current, effectively filtering out high-frequency components from the inverter's output. It smooths the current waveform, reducing high-frequency ripples. The capacitor C_n opposes changes in voltage, providing a path for high-frequency components to ground and smoothing the voltage waveform [33]. By applying all-pass filter to (4) and (5), the dynamic can be obtained as β-signals as follows.

$$i_o^\beta(t) = L_n^{-1}v^{\beta n}(t) - L_n^{-1}v_o^\beta(t) \tag{6}$$

$$\dot{v}_o^\beta(t) = C_n^{-1}i^\beta(t) - C_n^{-1}i_o^\beta(t) \tag{7}$$

To conveniently use integral control in this proposed control, the dynamic (4)-(7) should be converted to dq-frame model. The dq-frame transformation is an essential tool in power electronics and motor control [34]. It simplifies the operation of AC systems by converting complex AC waveforms into controllable DC-like signals. This enables the implementation of control schemes that are easier to understand and more accurate, hence enhancing the performance and efficiency of the system. Therefore, the model can be transformed using Clarke transformation with angular frequency ω as [26], [35]-[37]:

$$\dot{x}(t) = A_t x(t) + B_t u(t) + E_t i_o^{dq}(t) \tag{8}$$

Where $A_t = \begin{bmatrix} 0 & \omega & -L_n^{-1} & 0 \\ -\omega & 0 & 0 & -L_n^{-1} \\ C_n^{-1} & 0 & 0 & \omega \\ 0 & C_n^{-1} & -\omega & 0 \end{bmatrix}$, $B_t = \begin{bmatrix} L_n^{-1} & 0 \\ 0 & L_n^{-1} \\ 0 & 0 \\ 0 & 0 \end{bmatrix}$, $E_t = \begin{bmatrix} 0 & 0 \\ 0 & 0 \\ -C_n^{-1} & 0 \\ 0 & -C_n^{-1} \end{bmatrix}$, $x(t) = \begin{bmatrix} i^d(t) \\ i^q(t) \\ v^d(t) \\ v^q(t) \end{bmatrix}$, $u(t) = \begin{bmatrix} v^{dn}(t) \\ v^{qn}(t) \end{bmatrix}$, and $i_o^{dq}(t) = \begin{bmatrix} i_o^d(t) \\ i_o^q(t) \end{bmatrix}$.

Generally, the characteristic of the inverter is in discrete-time function. Therefore, the continuous-time model (8) should be converted to discrete-time model with the sampling time h using Euler's approximation as:

$$x[k+1] = Ax[k] + Bu[k] + Ei_o^{dq}[k] \tag{9}$$

Where $B = hB_t$, $E = hE_t$, $A = I_{4\times4} + hA_t$, and $I_{4\times4}$ is fourth order identity matrix.

The design element of this proposed robust control is considering uncertainties of the system in case of parameter variation within predetermined range. Additionally, uncertainty range directly affects the system's performance by influencing the trade-off between robustness and performance. A wider uncertainty range requires a more robust controller but can lead to overly conservative behavior and poor performance. Conversely, a too narrow uncertainty range may result in instability or performance degradation due to inadequate robustness. The robust control gain will be computed to guarantee the stability under parameter variation from lower to upper bounce. The capacitance and inductance value of the LC-filter are considered as the system parameters and their range are determined as follows.

$$L_l < L_n < L_u \tag{10}$$

$$C_l < C_n < C_u \tag{11}$$

or equivalent to

$$L_n/\varepsilon < L_n < \varepsilon L_n \tag{12}$$

$$C_n/\varepsilon < C_n < \varepsilon C_n \tag{13}$$

Where ε (>1) denotes uncertainty range and can be use as and performance tuning parameter. When the parameters vary under uncertain range (12) and (13) the system will change as well. Thus, the system model will have four possible uncertain sets (A_i, B_i) corresponding to the pair of (A, B); where (i = 1, 2, 3, 4). The uncertain pair of matrices (A_i, B_i) can be determined as [38]:

$$\Lambda = \left\{ \sum_{i=0}^{4} \varepsilon_i (A_i, B_i) \middle| \sum_{i=0}^{4} \varepsilon_i = 1, \varepsilon_i \geq 0 \right\} \tag{14}$$

Or equivalent to

$$(A_1, B_1) = \left(\begin{bmatrix} 1 & h\omega & -hL_l^{-1} & 0 \\ -h\omega & 1 & 0 & -hL_l^{-1} \\ hC_l^{-1} & 0 & 1 & h\omega \\ 0 & hC_l^{-1} & -h\omega & 1 \end{bmatrix}, h \begin{bmatrix} L_l^{-1} & 0 \\ 0 & L_l^{-1} \\ 0 & 0 \\ 0 & 0 \end{bmatrix} \right) \tag{15}$$

$$(A_2, B_2) = \left(\begin{bmatrix} 1 & h\omega & -hL_l^{-1} & 0 \\ -h\omega & 1 & 0 & -hL_l^{-1} \\ hC_u^{-1} & 0 & 1 & h\omega \\ 0 & hC_u^{-1} & -h\omega & 1 \end{bmatrix}, h \begin{bmatrix} L_l^{-1} & 0 \\ 0 & L_l^{-1} \\ 0 & 0 \\ 0 & 0 \end{bmatrix} \right) \tag{16}$$

$$(A_3, B_3) = \left(\begin{bmatrix} 1 & h\omega & -hL_u^{-1} & 0 \\ -h\omega & 1 & 0 & -hL_u^{-1} \\ hC_l^{-1} & 0 & 1 & h\omega \\ 0 & hC_l^{-1} & -h\omega & 1 \end{bmatrix}, h \begin{bmatrix} L_u^{-1} & 0 \\ 0 & L_u^{-1} \\ 0 & 0 \\ 0 & 0 \end{bmatrix} \right) \tag{17}$$

$$(A_4, B_4) = \left(\begin{bmatrix} 1 & h\omega & -hL_u^{-1} & 0 \\ -h\omega & 1 & 0 & -hL_u^{-1} \\ hC_u^{-1} & 0 & 1 & h\omega \\ 0 & hC_u^{-1} & -h\omega & 1 \end{bmatrix}, h \begin{bmatrix} L_u^{-1} & 0 \\ 0 & L_u^{-1} \\ 0 & 0 \\ 0 & 0 \end{bmatrix} \right) \tag{18}$$

The uncertainty models (15)-(16) are used in gain determining procedure so that the stability can be guaranteed withing this predetermined range [39], [40]. The uncertainty range ε is initially selected as a number close to 1, i.e., 1.1. To eliminate high overshoot and provide an acceptable transient response, it is advisable to choose a wider range until no overshoot occurs.

3. LMI-Based Robust Tracking Control

The proposed robust control system utilizes a state feedback control technique with integrated action to ensure stability and provide offset-free results [41]. The controller can be outlined as follows:

$$\begin{cases} i[k] = i[k-1] + e[k] \\ u[k] = K_x x[k] + K_i i[k] \end{cases} \tag{19}$$

Where error state $e[k] = v_{ref} - Cx[k]$, $C = \begin{bmatrix} 0 & 0 & 1 & 0 \\ 0 & 0 & 0 & 1 \end{bmatrix}$, $x[k]$ is the system state, reference state $v_{ref} = \begin{bmatrix} v_{ref} 0 \end{bmatrix}^T$, $i[k]$ denotes discretized integral states, $u[k]$ is the control input, K_x represents the state feedback control gain, and K_i is integral control gain. To determine the robust control gain K_x and K_i of this proposed system a systematic and step by step process is discussed in this section. The system state and integral state can be augmented as:

$$f[k+1] = \Gamma f[k] + \Psi u[k] + \Theta[k] \tag{20}$$

where $f[k] = \begin{bmatrix} x[k] \\ i[k] \end{bmatrix}$, $\Gamma = \begin{bmatrix} A & 0_{4\times2} \\ -C & I_{2\times2} \end{bmatrix}$, $\Psi = \begin{bmatrix} B \\ 0_{2\times2} \end{bmatrix}$, $\Theta[k] = \begin{bmatrix} E i_o^{dq}[k] \\ v_{ref} \end{bmatrix}$.

The control input of this augmented system can be defined as:

$$u[k] = Kf[k] \text{ where } (K = [K_x K_i]). \tag{21}$$

Replacing control input (21) in (20), the closed-loop dynamics can be obtained as assuming that $\Theta[k]$ is zero to obtain the robust control gain:

$$f[k+1] = (\Gamma + \Psi K) f[k] \tag{22}$$

Using Lyapunov function, the closed-loop dynamics (22) stable if the condition bellow is satisfied:

$$(\Gamma + \Psi K)^T W (\Gamma + \Psi K) - W < -(1 - \gamma^2) W \tag{23}$$

In this context, $\gamma (0 < \gamma < 1)$ represents the factor of convergence, and W is a positive definite matrix. Then, applying the Schur's complement to (23) to attain the linear matrix inequality form as:

$$\begin{bmatrix} \gamma^2 W & (\Gamma + \Psi K)^T \\ \Gamma + \Psi K & W^{-1} \end{bmatrix} > 0 \tag{24}$$

or equivalent to

$$\begin{bmatrix} \gamma^2 M & (\Gamma M + \Psi N)^T \\ \Gamma M + \Psi N & M \end{bmatrix} > 0 \tag{25}$$

where $M := W^{-1}$ and $N = KM$. To provide robustness to the system, the uncertainty model should be included in the LMI [42]-[45]. In order to incorporate the uncertainty model to the robust control design, the inequality (25) can be rewritten with the possible sets (15)-(18) as follows:

$$\begin{bmatrix} \gamma^2 M & (\Gamma_i M + \Psi_i N)^T \\ \Gamma_i M + \Psi_i N & M \end{bmatrix} > 0 \tag{26}$$

where $\Gamma_i := \begin{bmatrix} A_i & 0_{4\times2} \\ -C & I_{2\times2} \end{bmatrix}$, $\Psi_i := \begin{bmatrix} B_i \\ 0_{2\times2} \end{bmatrix}$, and ($i$ = 1,2,3,4).

To expedite the stabilization of the output voltage, it is recommended to select the value of γ that minimizes M while adhering to the LMI condition (22). Thus, the optimization problem can be defined as.

$$\underset{\gamma,N}{Minimize} \quad M \quad \text{subject to (26)} \tag{27}$$

To solve this generalized eigenvalue problem, use the YALMIP toolbox following the clear information in reference [46]. The robust optimal gain can be represented as:

$$K = NM^{-1} \tag{28}$$

The controller derived from solving equation (27) ensures that the monotonicity criterion is satisfied, ensuring overall stability against any perturbations in parameters L_n and C_n within the specified uncertainty range [47]-[49]. In addition, the YALMIP toolbox can be obtained by downloading it from https://yalmip.github.io/. The website provides detailed and comprehensive guidance along with instructions on how to deal with this optimization problem using MATLAB.

It should be noted that this proposed method provides less complexity in implementing the algorithm due to the predetermined gain using YALMIP. The robust stabilizing gain is then used in control algorithms without the need of real-time optimization problem solving like the MPC method. Therefore, this proposed approach utilizes significantly lower computational power in comparison to MPC.

The experimental setup for a single-phase inverter using Space Vector Pulse Width Modulation (SVPWM) includes several key components and steps. The inverter consists of Insulated Gate Bipolar Transistors (IGBTs) arranged in an H-bridge configuration. The H-bridge consists of four IGBTs connected such that each leg of the bridge has two IGBTs in series, and the midpoints of these legs are connected to the load as shown in Fig. 2. This setup allows for the conversion of DC power to AC power by controlling the switching of the IGBTs. An LC-filter, comprising an inductor and a capacitor, is connected to the output of the H-bridge to smooth the current ripple and reduce harmonic distortion. A TMS320F28335 Digital Signal Processor (DSP) is used to implement the SVPWM algorithm in real-time. The DSP generates PWM signals that control the switching of the IGBTs in the H-bridge.

Voltage and current sensors are connected to the output of the inverter to measure the output voltage and current, providing feedback to the DSP controller. An Analog-to-Digital Converter (ADC) integrated within the DSP converts these analog sensor signals to digital for processing. A DC source is connected to the input of the H-bridge to provide the necessary DC voltage. A resistive load is connected to the output of the LC-filter to test the inverter output under different load steps.

Software tools which is Code Composer Studio is used for programming the SVPWM algorithm on the DSP, while MATLAB helps compute the robust control gain before hardware implementation. Measurement instruments, including an oscilloscope and power analyzer are used to observe the inverter output waveform, measure total harmonic distortion (THD), output power, and efficiency, and log real-time data for analysis.

4. Results and Discussion

4.1. Simulations

The results of the simulation involve the utilization of MATLAB to calculate the stabilizing gain for the closed-loop system (20) with the uncertainty set (14). Next, the set of gains is implemented on the dynamic-links library (dll) using the C program in Microsoft Visual Studio. The dll block in PSIM is utilized to acquire simulation findings. Table 1 displays the parameters of the system utilized in the

simulation, while the control structure of this proposed method is shown in Fig. 3. The simulation uses an uncertainty range of $\varepsilon = 1.8$.

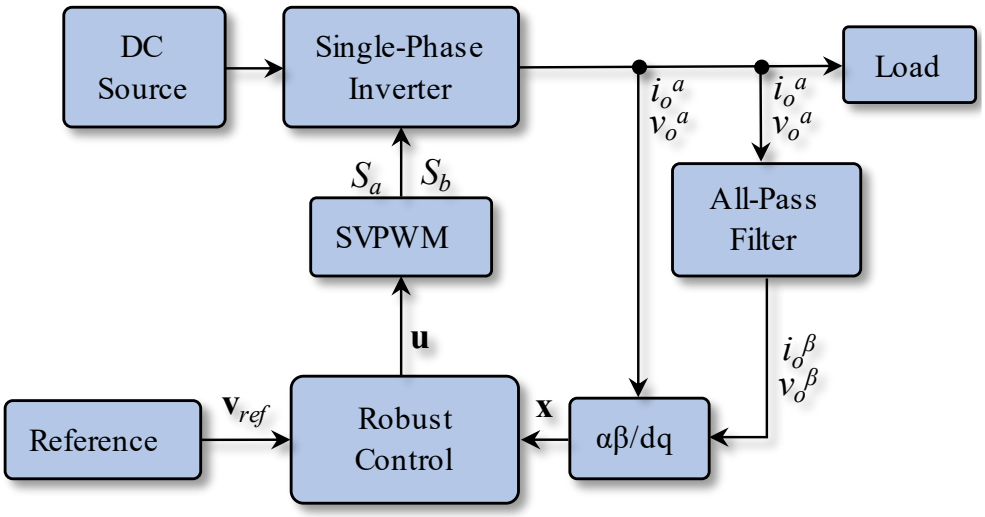

Fig. 3. Single-phase inverter proposed control structure

Table 1. Parameters of the system for simulations

Descriptions	Notation	Values
Inductance of filter	L_n	5 mH
Capacitance of filter	C_n	50 µF
DC source	V_{dc}	380 V
Sampling period	h	0.1 ms
Voltage reference	v_{ref}	156V(max)
Angular frequency	ω	100π (50 Hz)
Resistive load (Step 1)		150 Ω
Resistive load (Step 2)		75 Ω
Resistive load (Step 3)		50 Ω

The β-voltage can be generated by applying digital all-pass filters (APF) to the original signals, which shifts the phase by 90 degrees. The result obtained utilizing the APF is shown in Fig. 4. The horizontal axis represents time in seconds, ranging from 0 to approximately 0.12 seconds, while the vertical axis denotes voltage in volts. It is important to note that while APF can generate the β-voltage, the transient component initially causes interference with the dq-frame signals. Therefore, the dq-frame voltage is not entirely pure, resulting in a little oscillation in the transient part.

Fig. 5 represents the output voltage of the single-phase inverter, which has a reference value of 156V. During the time interval from t = 0s to t = 0.06s, the resistive load of 150Ω is applied. Subsequently, an additional load of 150Ω is connected in parallel. The simulation demonstrates highly satisfactory and rapid performance in restoring the output voltage at t = 0.06s, with no deviation from the desired value in the steady state. Fig. 6 shows the output current, with the same loading as Fig. 5. The performance remains stable despite the abrupt change in output loads.

Fig. 7 exhibits the output performance of the inverter voltage in the dq-frame. The initial value at t = 0 is approximately 0 V, and the steady-state value is around 156 V. The rise time is defined as the time taken for the waveform to go from 10% to 90% of its final value. In this case, 10% of 156 V is 15.6 V, and 90% is 143.1 V. The v_d reaches 15.6 V at around 0.002 seconds and 143.1 V at around 0.005 seconds. Thus, the rise time is approximately 0.003 seconds (3 ms). Both v_d and v_q show significant transient behavior within the first 0.02 seconds, characterized by rapid changes and oscillations. Then, both voltages reach a steady state relatively quickly. The v_d component stabilizes at around 156 V, while v_q settles at 0 V, indicating effective decoupling and control in the dq-frame. The oscillations in the v_q component indicate underdamping, but it successfully stabilizes without

sustained oscillations. As previously stated, the transient components of both the d- and q-axes present notable oscillations due to their use of the all-pass filter. Nevertheless, the proposed technique consistently maintains a stable overall performance, demonstrating excellent tracking capabilities.

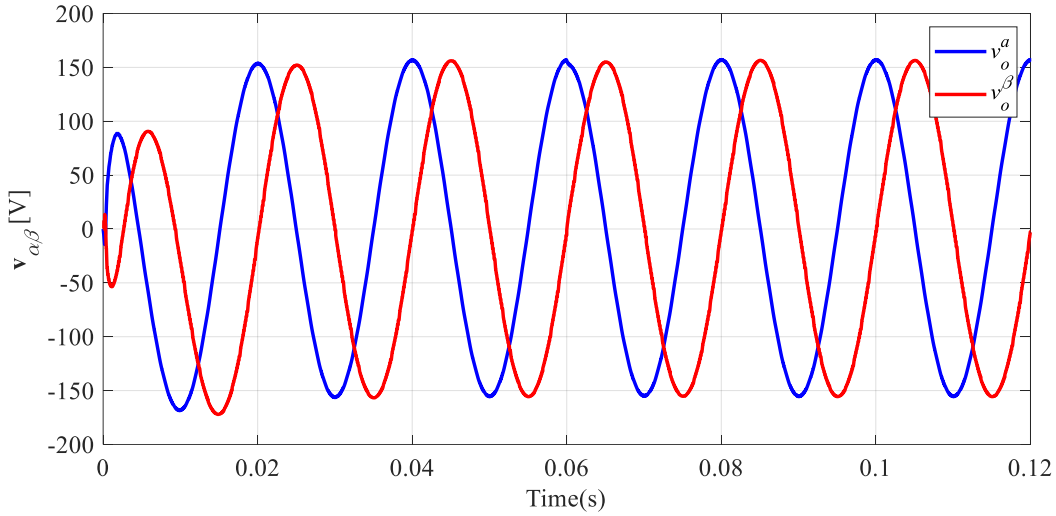

Fig. 4. AC output voltage with generated β-voltage using APF with the reference of 156V

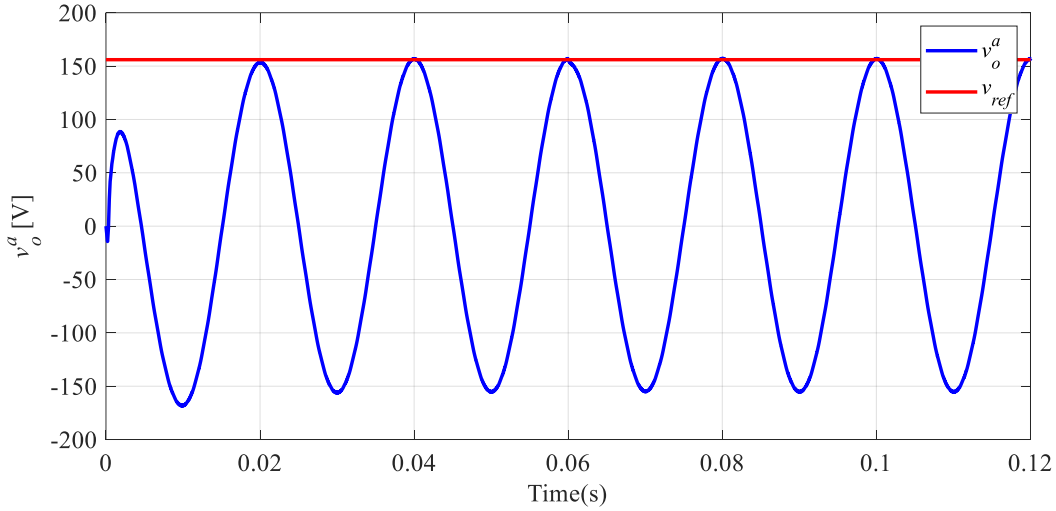

Fig. 5. Output AC voltage in *abc*-frame with reference value

Fig. 8 discusses several choices for uncertainty ranges. The performance of simulations employing ε values of 1.0, 1.5, 1.8, and 2.5 has been compared in this figure. All waveforms show initial oscillations before settling to their steady-state values. The *d*-axis voltage components (upper set of waveforms) exhibit significant overshoot initially, with the amplitude around 156 V, while the *q*-axis voltage components (lower set of waveforms) stabilize around 0 V. The rise time, or the time taken for each waveform to reach from 10% to 90% of its final value, varies with ε. The rise times are approximately 0.004 seconds for ε = 1.0, 0.003 seconds for ε = 1.5, and 0.0025 seconds for both ε = 1.8 and ε = 2.5. The settling time, defined as the time taken to remain within 2% of the final value, also varies. The settling times are approximately 0.06 seconds for ε = 1.0, 0.05 seconds for ε = 1.5, 0.045 seconds for ε = 1.8, and 0.04 seconds for ε = 2.5. This graph provides insights into how varying ε affects system stability and response time, aiding in optimal control system design. In summary, the uncertainty range ε = 1.8 can be regarded as the ideal tuning parameter for this single-phase inverter system, since it delivers outstanding performance in comparison to other values.

Fig. 9 displays the results of both the proposed approach and PI control. At time t = 0s, the output side of the resistive load *R*, which has a resistance of 150Ω, is connected. Following that, a second

resistive load with a resistance of 150Ω is connected in parallel at a time of 0.6s. The graph displays the transient responses of dq-axis voltage components for different control settings: proposed control with $\varepsilon = 1.8$ (blue), PI 1 (green), and PI 2 (red). The blue waveform ($\varepsilon = 1.8$) shows moderate overshoot and settles around 0.04 seconds. The green waveform (PI 1) exhibits higher overshoot and longer settling time of about 0.06 seconds, indicating less desirable performance. In addition, the red waveform (PI 2) has a smoother response with less overshoot and a quicker settling time of approximately 0.045 seconds, reflecting a more efficient control setting compared to PI 1. This analysis highlights how different control parameters influence system performance, with the proposed showing the most desirable results in terms of stability and rapid settling. Furthermore, the proposed controller demonstrates consistent performance across various load steps due to its robust nature. Nevertheless, the PI controller faces difficulties in maintaining good performance over varying load steps.

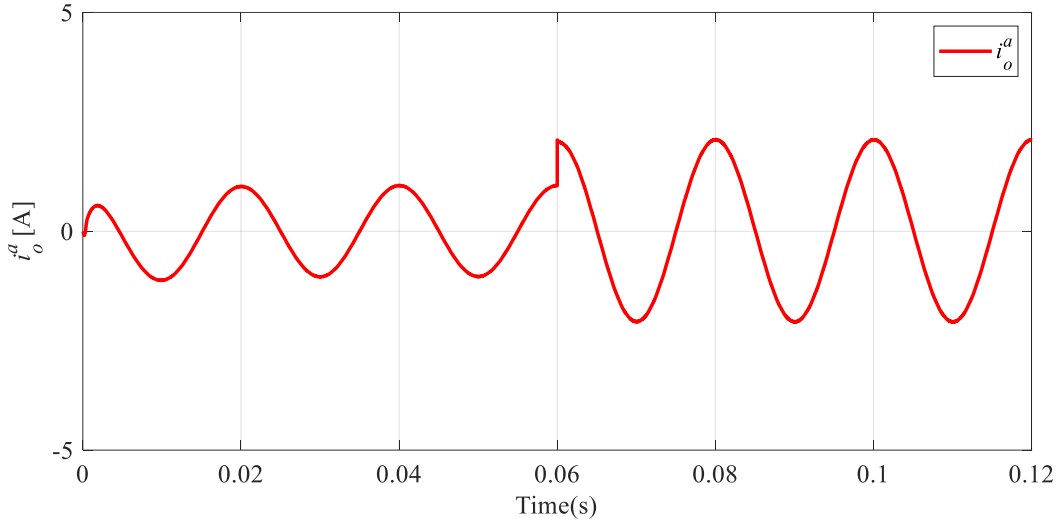

Fig. 6. Output current with second load steps at t = 0.06s

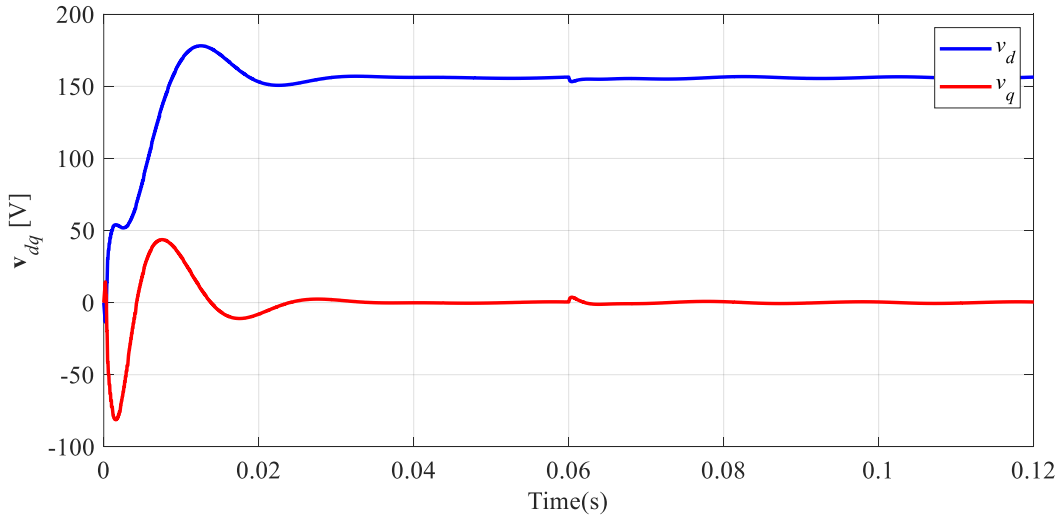

Fig. 7. Transient performance of the output voltage in dq-frame

Overall, compared to PI control, the proposed approach demonstrates robust performance in various load steps. Furthermore, the method's systematic control design allows for straightforward gain computation and results in optimal performance. The range of uncertainty can be utilized for the purpose of performance fine-tuning. Increasing the range of ε causes the inverter's performance to slow down. Conversely, employing a narrower range of ε leads to a faster transient response.

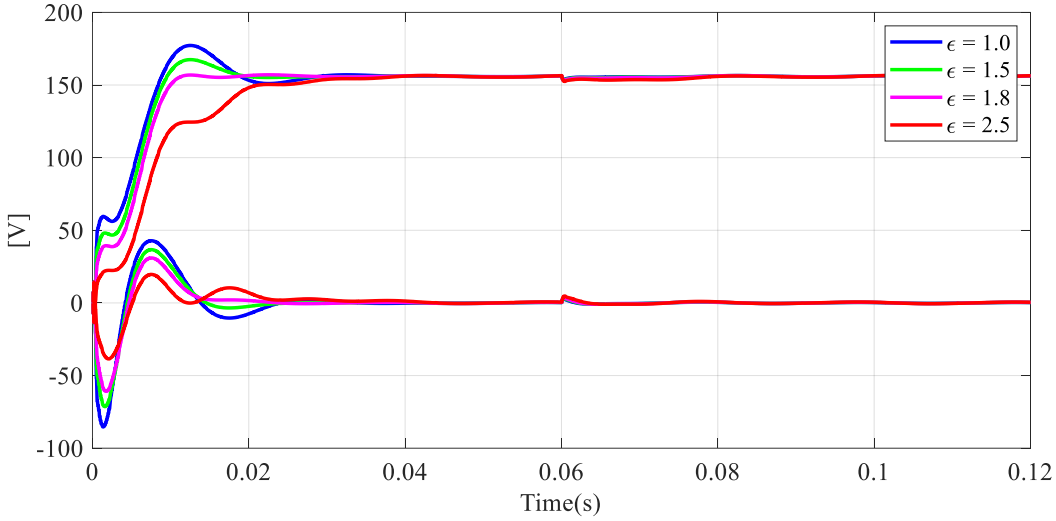

Fig. 8. Output voltage in dq-frame using different type of uncertainty range ε

It is worth noting that the proposed method utilizes digital all-pass filters to produce artificial signals, enabling control of the inverter in the dq-frame. This causes the initial oscillation at the transient part of the output in the dq-frame, as seen in Fig. 4. One possible solution to this is to create ideal β-signals as quickly as possible, without the transient effect. Until now, there has been no method to tackle this problem. However, such small oscillations at the transient part have no great impact on the overall performance of the inverter. According to Fig. 7, as the output stabilizes, the load disturbance at t = 0.06s does not significantly affect the overall performance. Fig. 9 demonstrates that the proposed technique exhibits more resilience and less ripple in comparison to the PI control.

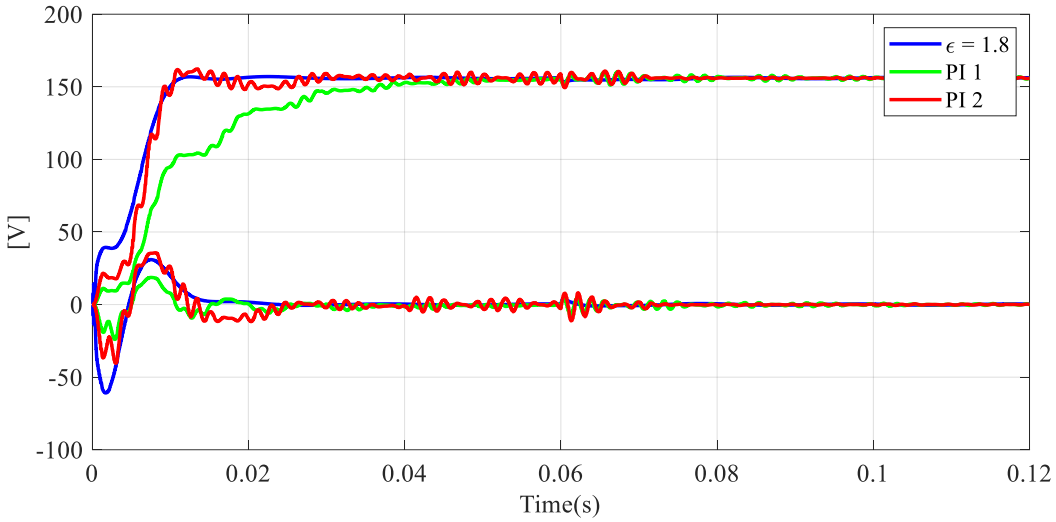

Fig. 9. Output voltage in dq-frame comparing to conventional PI control

4.2. Experimental Results

The experimental results utilize identical parameters to those employed in the simulation, as presented in Table 1. The experimental configuration is outlined in Fig. 10, while the whole set of hardware can be seen in Fig. 11. The control algorithm is carried out by utilizing a control board equipped with a TMS320F28335 signal processor, operating at a sampling frequency of 10 kHz. The experiment utilizes the identical gain as observed in the simulation, ensuring its robustness. The Rigol DS1204B Oscilloscope is used to measure the output voltage, while a Kyoritsu KEW 6315 Power Analyzer is used to measure the total harmonic distortion (THD). Because of the absence of measuring hardware, it is not possible to obtain the dq-frame signals experimentally. Instead, the AC signals are

measured and discussed using various load steps. It is worth noting that the robust gain used in the simulation is identical to the experiments. However, the performance of the simulation and experiment is slightly different, specifically the transient speed. The experiment is significantly slower. This may happen due to the measuring noise and the real nature of the parameters which not ideal or constant.

Initially, the inverter was operated without any load connected to its output side. Following that, the initial load step with a resistance of 150Ω is connected as shown in Fig. 12. The transient response of the inverter is very swift, exhibiting excellent reference tracking. Additionally, the THD of the output voltage at the first load step is presented in Fig. 13. High THD in an inverter system leads to increased power losses, reduced efficiency, overheating, and mechanical stress on connected equipment, thereby decreasing overall system reliability and lifespan [50]. Minimizing THD is essential to ensure efficient power delivery and the smooth operation of sensitive electronic devices. The THD is measured as 1.01% using the Power Analyzer, which is within an acceptable range. The second load step is then connected in parallel, resulting in a total resistance of 75Ω. Similarly, the inverter's performance remains nearly unchanged compared to the initial load step, as confirmed in Fig. 14. However, the THD of the output voltage exhibits a minor rise to 1.28%, as indicated in Fig. 15. Eventually, the last step is connected parallelly resulting in a total resistance of 50Ω. The performance of the inverter is consistent with both transient and steady state, as depicted in Fig. 16. In Fig. 17, the voltage THD advances to 1.61%.

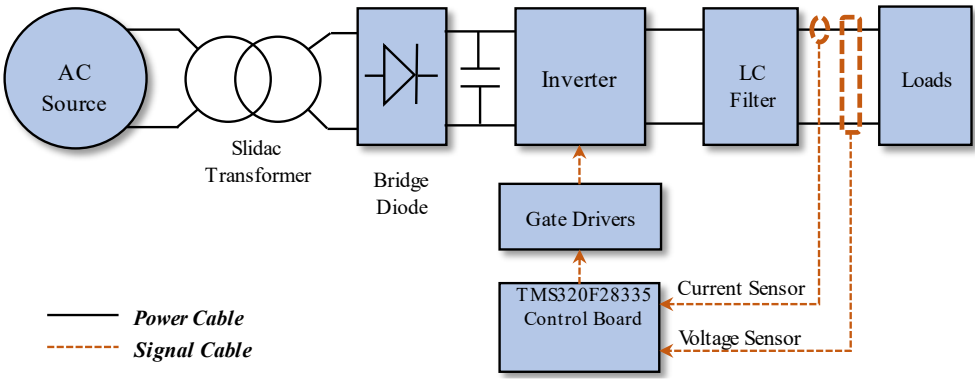

Fig. 10. Experimental configuration

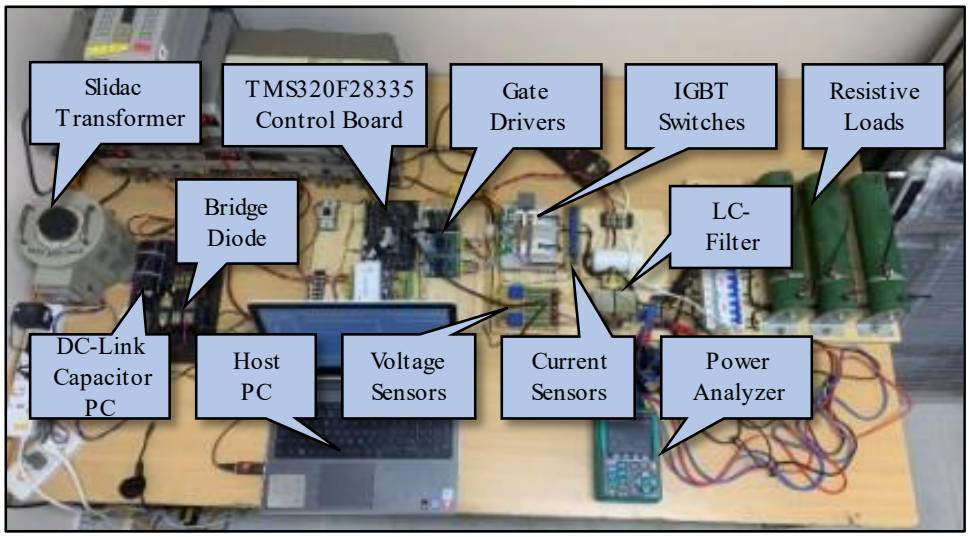

Fig. 11. Experimental setup

The PI control was implemented using identical scenarios to ensure a fair comparison. The output voltage of the PI controller is fine-tuned until it demonstrates satisfactory performance. It is important to note that gain tuning is a significant challenge when implementing a PI controller, requiring

substantial time and efforts to achieve satisfactory performance. The THD of the output voltage, when utilizing PI control, is shown in Fig. 18 for a load resistance of 150Ω, in Fig. 19 for a load resistance of 75Ω, and in Fig. 20 for a load resistance of 50Ω. It is evident that the proposed technique has superior performance compared to PI at each load step. The summarized results of THD for both controllers are presented in Table 2. The overall THD in each load step of the proposed control is significant lower compared to those of PI. It is 0.82% lower under load Step 1, 1.12% lower under load Step 2 and 3.46% lower under load Step 3.

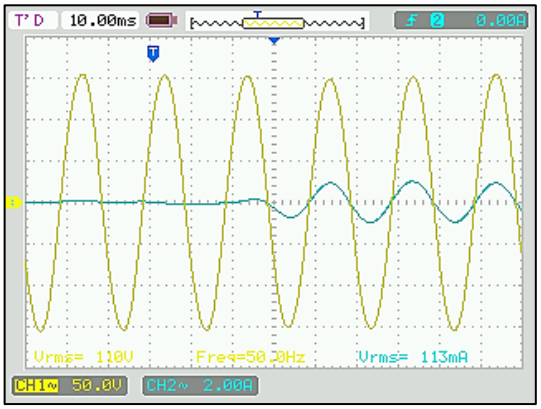

Fig. 12. Output voltage and current using 150Ω load step

Fig. 13. Voltage THD using 150Ω load step

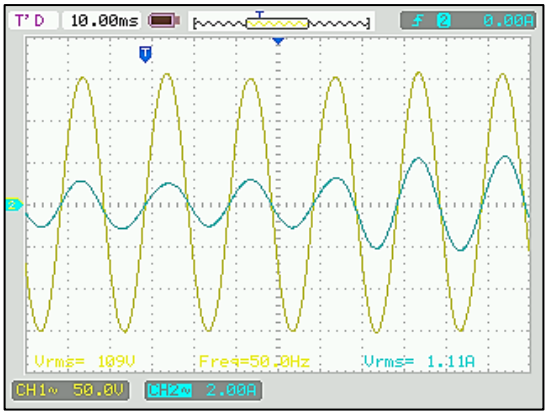

Fig. 14. Output voltage and current using 75Ω load step

Fig. 15. Voltage THD using 75Ω load step

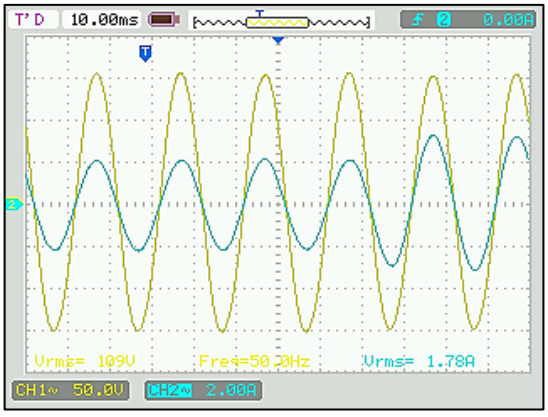

Fig. 16. Output voltage and current using 50Ω load step

Fig. 17. Voltage THD using 50Ω load step

Fig. 18. Voltage THD under 150Ω load using PI control

Fig. 19. Voltage THD under 75Ω load using PI control

Fig. 20. Voltage THD under 50Ω load using PI control

Fig. 21. Summarized THD of the proposed method and PI control

Load Step	Robust Control THD	PI Voltage THD
Step 1: 150Ω	1.10%	1.92%
Step 2: 75Ω	1.28%	2.40%
Step 3: 50Ω	1.61%	5.07%

While the experimental results demonstrate that the proposed approach yields a lower THD in comparison to the PI control, this work does not address the transient performance of either control. This is due to the absence of the necessary hardware for acquiring the data from the control board. The control board utilized in the experiment is currently undergoing an upgrade to incorporate a controller area network (CAN) for future research purposes. The results can be evaluated in greater depth with the data captured from the control board. With the same reason, another noteworthy limitation of the experiments is that the study does not include the RL-load and non-linear load, which are quite common in real-life UPS systems. Additionally, it is important to mention that there was a presence of measurement noise in the output current and voltage during the experiment for both controllers, resulting in voltage ripple at the output. The presence of measurement noise can be effectively mitigated by employing a disturbance observer.

5. Conclusion

A robust control approach has been introduced for a single-phase inverter with an output filtered by an LC-filter. A key challenge in controlling single-phase power converters is the lack of a direct

method for transforming single-phase signals into dq-frame signals. By utilizing an all-pass filter in this proposed method, it becomes achievable to regulate the output voltage with regard to the DC quantity or the dq-rotating frame. Moreover, ensuring voltage stability and minimizing THD are important priorities when designing a UPS inverter. An optimization technique based on LMI is employed to determine the stabilizing gains of the controllers. The optimization criterion is to maximize the pace at which the system converges to a steady state, even in the presence of uncertainties. This approach offers a systematic approach to designing controllers by minimizing the need for tuning gain and ensuring stable performance even when there is uncertainty in the parameters. By choosing the uncertainty range ε, the controller demonstrates outstanding performance in both transient and steady states. Both simulation and experimental results prove that the proposed control has superior performance to the PI control in terms of THD. The THD of this proposed method is 0.82% lower under load Step 1, 1.12% lower under load Step 2 and 3.46% lower under load Step 3 compared to those of PI.

The proposed method uses digital all-pass filters to generate artificial signals for controlling the inverter in the dq-frame, causing initial oscillations during the transient phase. A potential solution is to generate ideal β-signals quickly to avoid this oscillation, though no such approach currently exists. Despite minor transient oscillations, the inverter's overall performance remains largely unaffected. Experimental results show a lower Total Harmonic Distortion (THD) with the proposed method compared to PI control, but transient performance was not studied due to a lack of data acquisition hardware on the control board. This board is being upgraded to include a Controller Area Network (CAN) for future research, allowing for a more thorough evaluation. The experiments also did not test RL-load and non-linear load, common in real-life UPS systems.

Additionally, it is important to mention that there was a presence of measurement noise in the output current and voltage during the experiment for both controllers, resulting in voltage ripple at the output. The presence of measurement noise can be effectively mitigated by employing a disturbance observer. Future studies will focus on integrating a disturbance observer to eliminate measurement noise in the inverter's voltage and current.

Author Contribution: All authors contributed equally to the main contributor to this paper. All authors read and approved the final paper.

Funding: This research received no external funding.

Acknowledgment: This work is supported by Love and Prayer Scholarship and the National Polytechnic Institute of Cambodia.

Conflicts of Interest: The authors declare no conflict of interest.

References

[1] H. Tang, B. So, S. In, P. Soth, S. Yay and C. Choeung, "Single-Phase UPS Inverter Using Offset-Free Optimizing Control with Digital All-Pass Filter," *2023 International Conference on Advanced Mechatronics, Intelligent Manufacture and Industrial Automation (ICAMIMIA)*, pp. 156-160, 2023, https://doi.org/10.1109/ICAMIMIA60881.2023.10427840.

[2] T. Kawabata, T. Miyashita and Y. Yamamoto, "Dead beat control of three phase PWM inverter," *IEEE Transactions on Power Electronics*, vol. 5, no. 1, pp. 21-28, 1990, https://doi.org/10.1109/63.45996.

[3] P. Mattavelli, "An improved deadbeat control for UPS using disturbance observers," *IEEE Transactions on Industrial Electronics*, vol. 52, no. 1, pp. 206-212, 2005, https://doi.org/10.1109/TIE.2004.837912.

[4] S. Ramaiah, N. Lakshminarasamma and M. K. Mishra, "An Improved Deadbeat Direct Power Control for Grid Connected Inverter System," *2021 IEEE 12th International Symposium on Power Electronics for Distributed Generation Systems (PEDG)*, pp. 1-6, 2021, https://doi.org/10.1109/PEDG51384.2021.9494243.

[5] P. Mattavelli, "A modified dead-beat control for UPS using disturbance observers," *2002 IEEE 33rd Annual IEEE Power Electronics Specialists Conference. Proceedings (Cat. No.02CH37289)*, pp. 1618-1623, vol. 4, 2002, https://doi.org/10.1109/PSEC.2002.1023042.

[6] S. Bayhan, H. Komurcugil and I. S. Bayram, "Deadbeat Control of a Three-Phase T-type Inverter with Output LC Filter for UPS Applications," *2021 IEEE 30th International Symposium on Industrial Electronics (ISIE)*, pp. 1-6, 2021, https://doi.org/10.1109/ISIE45552.2021.9576216.

[7] H. Ueta and T. Yokoyama, "Experimental Verification of Deadbeat Control with 1-MHz Multisampling and Disturbance Compensation Method for Three Phase PWM Inverter," *IEEJ Journal of Industry Applications*, vol. 8, no. 4, pp. 632–637, 2019, https://doi.org/10.1541/ieejjia.8.632.

[8] S. S. Seyedalipour, "A Novel Deadbeat Control for Three-Phase Grid-Connected VSI with an Output LCL Filter in Natural Frame," *2019 International Power System Conference (PSC)*, pp. 447-452, 2019, https://doi.org/10.1109/PSC49016.2019.9081546.

[9] X. Zhou, P. Huang, W. Yu, Y. Feng, Z. Qian and P. Yang, "The control strategy of Harmonic suppression of Photovoltaic grid-connected inverter based on PI+MPR," *2019 4th IEEE Workshop on the Electronic Grid (eGRID)*, pp. 1-5, 2019, https://doi.org/10.1109/eGRID48402.2019.9092748.

[10] H. Anantwar, S. Sundar, and B. R. Laksmikantha, "Optimal controllers design for voltage control in Off-grid hybrid power system," *International Journal of Electrical and Computer Engineering*, vol. 9, no. 6, pp. 4586-4597, 2019, https://doi.org/10.11591/ijece.v9i6.pp4586-4597.

[11] W. Chen, F. Cai, Q. Lin and W. Wang, "Improved PI and Repetitive Controller for Dual-Buck Inverter," *2020 39th Chinese Control Conference (CCC)*, pp. 6157-6161, 2020, https://doi.org/10.23919/CCC50068.2020.9188614.

[12] R. Wang, S. Wang, Z. Gong, M. Li, Y. Zhang and M. Huang, "Design of Single-phase Photovoltaic Inverter Based on Double Closed-loop PI and Quasi-PR Control," *2020 IEEE 2nd International Conference on Architecture, Construction, Environment and Hydraulics (ICACEH)*, pp. 80-82, 2020, https://doi.org/10.1109/ICACEH51803.2020.9366253.

[13] N. G. J. and M. N. B., "Current mode fractional order PID control of wind-based quadratic boost converter inverter system with enhanced time response," *Circuit World*, vol. 47, no. 4, pp. 368-381, 2021, https://doi.org/10.1108/CW-03-2020-0038.

[14] S. Li, W. Han, X. Li, and Z. Wang, "Harmonic Suppression Strategy of Photovoltaic Grid Connected Inverter Based on Repetitive and PI Control," *Journal of Physics: Conference Series*, vol. 2136, no. 1, p. 012032, 2021, https://doi.org/10.1088/1742-6596/2136/1/012032.

[15] P. Nithara and R. P. Eldho, "Comparative Analysis of Different Control strategies in Single phase Standalone Inverter," *2021 7th International Conference on Advanced Computing and Communication Systems (ICACCS)*, pp. 1105-1109, 2021, https://doi.org/10.1109/ICACCS51430.2021.9441547.

[16] D. Memije, O. Carranza, J. J. Rodríguez, R. Ortega, and E. Peralta, "Inverter harmonic perturbations rejection in renewable energy conversion systems applying a super-twisting algorithm," *IET Renewable Power Generation*, vol. 15, no. 7, pp. 1483-1497, 2021, https://doi.org/10.1049/rpg2.12128.

[17] R. Uthirasamy, V. Kumar Chinnaiyan, U. S. Ragupathy, and S. Vishnu Kumar, "Design and Implementation of Discrete Controller-Based Zeta Converter for Solar Power Applications," *Proceedings of International Conference on Power Electronics and Renewable Energy Systems*, vol. 795, pp. 61-69, 2022, https://doi.org/10.1007/978-981-16-4943-1_7.

[18] R. Uthirasamy *et al*., "Design of modified reference phase modulation based boost chopper fed fifteen level stepped DC link hybrid converter," *Scientific Reports*, vol. 14, no. 1, p. 2706, 2024, https://doi.org/10.1038/s41598-024-52727-8.

[19] C. Choeung, M. Leang Kry, and Y. Il Lee, "Robust Tracking Control of a Three-phase Charger under Unbalanced Grid Condition," *IFAC-PapersOnLine*, vol. 51, no. 28, pp. 173-178, 2018, https://doi.org/10.1016/j.ifacol.2018.11.697.

[20] A. Sahli, F. Krim, A. Laib, and B. Talbi, "Model predictive control for single phase active power filter using modified packed U-cell (MPUC5) converter," *Electric Power Systems Research*, vol. 180, p. 106139, 2020, https://doi.org/10.1016/j.epsr.2019.106139.

[21] A. M. Mahfuz-Ur-Rahman, M. R. Islam, K. M. Muttaqi and D. Sutanto, "Model Predictive Control for a New Magnetic Linked Multilevel Inverter to Integrate Solar Photovoltaic Systems With the Power Grids," *IEEE Transactions on Industry Applications*, vol. 56, no. 6, pp. 7145-7155, 2020, https://doi.org/10.1109/TIA.2020.3024352.

[22] M. Easley, S. Jain, M. Shadmand and H. Abu-Rub, "Autonomous Model Predictive Controlled Smart Inverter With Proactive Grid Fault Ride-Through Capability," *IEEE Transactions on Energy Conversion*, vol. 35, no. 4, pp. 1825-1836, 2020, https://doi.org/10.1109/TEC.2020.2998501.

[23] O. Gulbudak and M. Gokdag, "Finite control set model predictive control approach of nine switch inverter-based drive systems: Design, analysis, and validation," *ISA Transactions*, vol. 110, pp. 283–304, 2021, https://doi.org/10.1016/j.isatra.2020.10.037.

[24] M. Babaie, M. Sharifzadeh, M. Mehrasa, G. Chouinard and K. Al-Haddad, "Supervised Learning Model Predictive Control Trained by ABC Algorithm for Common-Mode Voltage Suppression in NPC Inverter," *IEEE Journal of Emerging and Selected Topics in Power Electronics*, vol. 9, no. 3, pp. 3446-3456, 2021, https://doi.org/10.1109/JESTPE.2020.2984674.

[25] M. C. Sha, R. J. Zhu, X. G. Yang, and X. Han, "Finite control set model predictive control of quasi-z-source inverter photovoltaic grid-connected," *Journal of Physics: Conference Series*, vol. 1748, no. 5, p. 052001, 2021, https://doi.org/10.1088/1742-6596/1748/5/052001.

[26] C. Choeung, H. Tang, P. Soth, V. Huy, and S. Srang, "LMI-Based Robust Voltage Regulation of a Single-Phase Inverter with LC-Filtered Output," *Computational Intelligence Methods for Green Technology and Sustainable Development*, vol. 567, pp. 314-324, 2023, https://doi.org/10.1007/978-3-031-19694-2_28.

[27] I. R. Fitri and J.-S. Kim, "A Nonlinear Model Predictive Control with Enlarged Region of Attraction via the Union of Invariant Sets," *Mathematics*, vol. 8, no. 11, p. 2087, 2020, https://doi.org/10.3390/math8112087.

[28] J. S. Lim, J.-S. Kim, and Y. I. Lee, "Robust tracking model predictive control for input-constrained uncertain linear time invariant systems," *International Journal of Control*, vol. 87, no. 1, pp. 120-130, 2014, https://doi.org/10.1080/00207179.2013.823669.

[29] I. R. Fitri, J. Kim, S. Yu, and Y. I. Lee, "Computation of Feasible and Invariant Sets for Interpolation-based MPC," *International Journal of Control, Automation and Systems*, vol. 19, pp. 3253-3263, 2021, https://doi.org/10.1007/s12555-021-0014-3.

[30] C. Choeung, M. L. Kry, and Y. Lee, "Robust Tracking Control of a Three-Phase Bidirectional Charger for Electric Vehicle," *Journal of Advanced Transportation*, 2022, https://doi.org/10.1155/2022/5077091.

[31] S. Yay, P. Soth, H. Tang, H. Cheng, S. Ang, and C. Choeung, "Power Regulation of a Three-Phase L-Filtered Grid-Connected Inverter Considering Uncertain Grid Impedance Using Robust Control," *International Journal of Robotics and Control Systems*, vol. 4, no. 2, pp. 779-794, 2024, http://dx.doi.org/10.31763/ijrcs.v4i2.1406.

[32] P. A. Regalia, S. K. Mitra and P. P. Vaidyanathan, "The digital all-pass filter: a versatile signal processing building block," *Proceedings of the IEEE*, vol. 76, no. 1, pp. 19-37, 1988, https://doi.org/10.1109/5.3286.

[33] J. Kim, J. Choi and H. Hong, "Output LC filter design of voltage source inverter considering the performance of controller," *PowerCon 2000. 2000 International Conference on Power System Technology. Proceedings (Cat. No.00EX409)*, vol. 3, pp. 1659-1664, 2000, https://doi.org/10.1109/ICPST.2000.898225.

[34] K. -N. Areerak, S. V. Bozhko, G. M. Asher and D. W. P. Thomas, "DQ-transformation approach for modelling and stability analysis of AC-DC power system with controlled PWM rectifier and constant power loads," *2008 13th International Power Electronics and Motion Control Conference*, pp. 2049-2054, 2008, https://doi.org/10.1109/EPEPEMC.2008.4635567.

[35] Y. Danayiyen, K. Lee, M. Choi, and Y. I. Lee, "Model Predictive Control of Uninterruptible Power Supply with Robust Disturbance Observer," *Energies*, vol. 12, no. 15, p. 2871, 2019, https://doi.org/10.3390/en12152871.

[36] V. Huy, H. Tang, P. Soth, S. Yay, K. Sovan and C. Choeung, "Three-phase Inverter using Robust Tracking Control based Interpolation," *2023 Third International Symposium on Instrumentation, Control,*

Artificial Intelligence, and Robotics (ICA-SYMP), pp. 91-95, 2023, https://doi.org/10.1109/ICA-SYMP56348.2023.10044739.

[37] Y. Danayiyen, İ. H. Altaş, and Y. I. Lee, "Robust Discrete Time Disturbance Observer with Finite Control Set Model Predictive Control in UPS System," *IFAC-PapersOnLine*, vol. 52, no. 4, pp. 51-56, 2019, https://doi.org/10.1016/j.ifacol.2019.08.154.

[38] J. S. Lim, C. Park, J. Han and Y. I. Lee, "Robust Tracking Control of a Three-Phase DC–AC Inverter for UPS Applications," *IEEE Transactions on Industrial Electronics*, vol. 61, no. 8, pp. 4142-4151, 2014, https://doi.org/10.1109/TIE.2013.2284155.

[39] I. R. Fitri, J. Kim, and H. Song, "A Robust Suboptimal Current Control of an Interlink Converter for a Hybrid AC/DC Microgrid," *Energies*, vol. 11, no. 6, p. 1382, 2018, https://doi.org/10.3390/en11061382.

[40] P. Soth, S. San, H. Cheng, H. Tang, V. Torn and C. Choeung, "Voltage Regulation of a Three-Phase PV-Connected Inverter Using LMI-Based Optimization," *2023 International Conference on Advanced Mechatronics, Intelligent Manufacture and Industrial Automation (ICAMIMIA)*, pp. 1-5, 2023, https://doi.org/10.1109/ICAMIMIA60881.2023.10427886.

[41] C. Choeung, M. L. Kry, and Y. I. Lee, "Robust Tracking Control of a Three-Phase Charger under Unbalanced Grid Conditions," *Energies*, vol. 11, no. 12, p. 3389, 2018, https://doi.org/10.3390/en11123389.

[42] C. Choeung, P. Soth, H. Tang, S. Ean, and S. Srang, "A Linear Matrix Inequality Approach to Optimal Voltage Control of a Three-Phase UPS Inverter under Unbalanced Loads," *Engineering Proceedings*, vol. 56, no. 1, p. 87, 2023, https://doi.org/10.3390/ASEC2023-15365.

[43] N. -B. Lai and K. -H. Kim, "Robust Control Scheme for Three-Phase Grid-Connected Inverters With LCL-Filter Under Unbalanced and Distorted Grid Conditions," *IEEE Transactions on Energy Conversion*, vol. 33, no. 2, pp. 506-515, 2018, https://doi.org/10.1109/TEC.2017.2757042.

[44] H. Tang *et al*., "Design of a Robust Control for a Single-Phase AC-DC Converter Using LMI Technique," *2023 International Electrical Engineering Congress (iEECON)*, pp. 1-5, 2023, https://doi.org/10.1109/iEECON56657.2023.10126791.

[45] P. Soth *et al*., "Robust Dual-Current Control of a Three-Phase Grid-Tied Inverter under Unbalanced Grid Voltage Using LMI Approach," *2023 International Electrical Engineering Congress (iEECON)*, pp. 6-11, 2023, https://doi.org/10.1109/iEECON56657.2023.10126574.

[46] J. Lofberg, "YALMIP: a toolbox for modeling and optimization in MATLAB," *2004 IEEE International Conference on Robotics and Automation (IEEE Cat. No.04CH37508)*, pp. 284-289, 2004, https://doi.org/10.1109/CACSD.2004.1393890.

[47] C. Choeung, S. H. Park, B. K. Koh, and Y. I. Lee, "Robust tracking control of a three-phase DC-AC inverter for UPS application under unbalanced load conditions," *IFAC-PapersOnLine*, vol. 49, no. 27, pp. 278-283, 2016, https://doi.org/10.1016/j.ifacol.2016.10.704.

[48] Jae Sik Lim and Young Il Lee, "Design of a robust controller for three-phase UPS systems using LMI approach," *International Symposium on Power Electronics Power Electronics, Electrical Drives, Automation and Motion*, pp. 654-657, 2012, https://doi.org/10.1109/SPEEDAM.2012.6264527.

[49] C. Choeung *et al*., "Linear Matrix Inequality-Based Optimal State Feedback Control of a Three-Phase L-filtered Grid-Connected Inverter," *2023 Third International Symposium on Instrumentation, Control, Artificial Intelligence, and Robotics (ICA-SYMP)*, pp. 135-139, 2023, https://doi.org/10.1109/ICA-SYMP56348.2023.10044932.

[50] A. Arranz-Gimon, A. Zorita-Lamadrid, D. Morinigo-Sotelo, and O. Duque-Perez, "A Review of Total Harmonic Distortion Factors for the Measurement of Harmonic and Interharmonic Pollution in Modern Power Systems," *Energies*, vol. 14, no. 20, p. 6467, 2021, https://doi.org/10.3390/en14206467.